Re-Os Ages of Group IIA, IIIA, IVA, and IVB Iron Meteorites

Michael I. Smoliar, Richard J. Walker,* John W. Morgan

Rhenium and osmium concentrations and osmium isotopic ratios of group IIA, IIIA, IVA, and IVB iron meteorites were determined by negative thermal ionization mass spectrometry with modified digestion and equilibration techniques. Precise isochrons are defined for all four groups. An absolute age of 4558 million years is assumed for group IIIA irons, leading to closure ages of 4537 ± 8, 4456 ± 25, and 4527 ± 29 million years for the group IIA, IVA, and IVB irons, respectively. The initial osmium-187/osmium-188 ratios of the IIA, IIIA, and IVA groups, as a function of crystallization age, suggest that the rhenium/osmium ratio of the parental materials to these asteroidal cores was similar to that of ordinary chondrites. Data for IVB irons, in contrast, indicate a different mode of formation and derivation from a distinctly nonchondritic osmium reservoir.

Most iron meteorites are presumed to represent fragments of the cores of small planetary bodies. They are distinguishable from other iron meteorites in that their compositions are consistent with crystal-liquid fractionation trends imparted during core crystallization from metallic magma (*1*, *2*). The term "magmatic irons" is used to describe such meteorites. The group IIA, IIIA, IVA, and IVB iron meteorites studied here are magmatic irons and make up about 90% of all magmatic irons.

Precise determination of the crystallization age of each iron meteorite group is critical to understanding the timing of parent body accretion, melting, segregation of metal into the core, and subsequent cooling. Such age constraints have been impossible to obtain because parent and daughter elements of conventional long-lived radiogenic isotope systems occur in very low abundances in metallic phases. Short-lived systems, such as ^{107}Pd-^{107}Ag and ^{53}Mn-^{53}Cr, permit some limitations to be placed on the postnucleosynthesis history of some irons (*3*–*7*).

Currently, the best long-lived radiogenic isotope system for dating iron meteorites is the Re-Os decay scheme {$^{187}\text{Re} \rightarrow {}^{187}\text{Os}$ by β decay; with a decay constant [$\lambda(^{187}\text{Re})$] of $\sim 1.64 \times 10^{-11}$ year^{-1}}. The system is useful because the highly siderophile elements, Re and Os, occur in relatively high concentrations in many iron meteorites, and the Re/Os ratio of the metallic melts varied significantly throughout the crystallization sequences of most magmatic iron groups. Consequently, it may be possible to determine high-precision isochrons for most groups. For example, using negative thermal ionization techniques, Horan *et al.* (*8*) obtained a group IIA isochron with an uncertainty of ±31 million years (My). Since then, advances in chemical equilibration and separation techniques have permitted the production of more precise Re-Os isochrons (*9*, *10*).

Despite improvements in analytical techniques, two problems hinder our ability to obtain precise Re-Os absolute ages: the ±3% uncertainty in $\lambda(^{187}\text{Re})$ (*11*), and deviations from stoichiometry in the Os metal standards, which are needed to accurately calibrate the enriched isotope spikes used for isotope dilution measurements (*12*). Both problems limit the accuracy of absolute ages calculated from Re-Os isochrons, but they do not prevent the system from being used to place precise relative age constraints. In this case, precision is limited only by isochron uncertainty, which is less than 0.5% (*9*, *10*).

Here, we assumed the group IIIA irons formed at about the same time as angrite meteorites, for which a crystallization age has been precisely determined [4557.8 ± 0.4 million years ago (Ma)] (*13*). Angrites have a well-constrained ^{53}Mn-^{53}Cr formation interval (*3*, *14*) that is within ±5 My of the ^{53}Mn-^{53}Cr formation interval reported for group IIIAB irons (*4*), suggesting that the above assumption is valid within the same time uncertainty (±5 My).

Here we have used a mixed Re-Os spike that was calibrated using previously established standards (*15*), and with these results (Table 1) we calculated ages for the iron groups (Table 2). Combining the angrite age of 4558 Ma and the slope of the IIIA isochron (Fig. 1A) gives a ^{187}Re decay constant of 1.666×10^{-11} year^{-1} (*16*). All the data for the IIA group also form a well-constrained isochron (Fig. 1B), in agreement with previously published slopes and initial ratios for IIA irons (*8*, *9*). The IIA and IIIA isochron slopes are resolvable and indicate that the IIA irons are younger (4537 ± 8 Ma) than the IIIA irons, although the difference in ages may be as little as 1 My (Table 2).

Group IVA irons show more complex Re-Os systematics: Seven irons define an apparent isochron with an age of 4456 ± 25 Ma that is distinctly younger than the ages of the IIA and IIIA groups; however, three additional irons (La Grange, Bushman Land, and Duel Hill) deviate significantly from this isochron (Fig. 1C). All three nonisochronous meteorites have isotopic compositions consistent with an older age. Rasmussen *et al.* (*17*) showed that the IVA parent body probably experienced a catastrophic impact soon after formation. Such an event could complicate the Re-Os record in this group by two mechanisms: impact resetting of the isotopic system, and

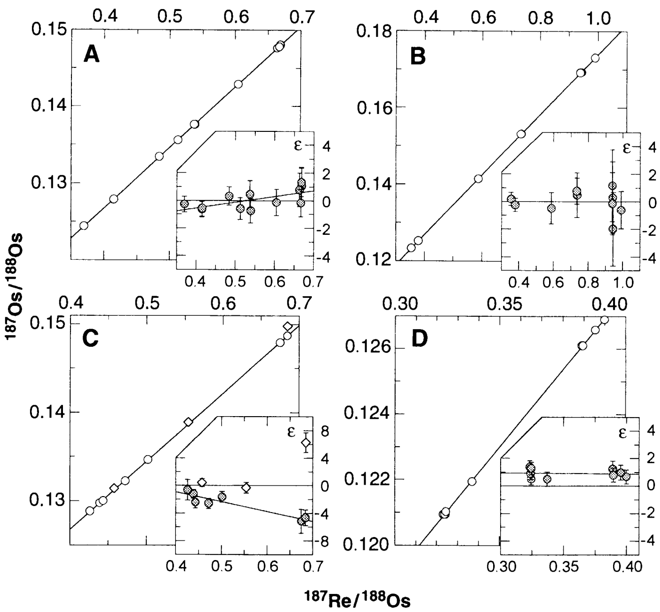

Fig. 1. Re-Os isochrons for (**A**) IIIA, (**B**) IIA, (**C**) IVA, and (**D**) IVB iron meteorites. The insets show the deviation in parts per 10,000 of data points from the best fit line in ε units: $\varepsilon = [(^{187}\text{Os}/^{188}\text{Os}) - S(^{187}\text{Re}/^{188}\text{Os} - I_O)] \times 10^4$, where S and I_O denote the isochron parameters of slope and initial ^{187}Os/^{188}Os ratio, respectively. For all meteorites, ε was calculated relative to the IIA isochron (represented by horizontal lines on the insets). Error bars on the insets account for uncertainties in both ^{187}Os/^{188}Os and ^{187}Re/^{188}Os ratios. The three IVA irons that were omitted in the isochron regression are shown as open diamonds.

M. I. Smoliar and R. J. Walker, Isotope Geology Laboratory, Department of Geology, University of Maryland, College Park, MD 20742, USA.
J. W. Morgan, Department of Earth Resources, Colorado State University, Fort Collins, CO 80523, USA.

---

*To whom correspondence should be addressed.

the possible mixing of two different metal sources. Concentrations of Re and Os in IVA samples plot on a linear trend of logarithm [Re] versus logarithm [Os], consistent with fractional crystallization (Fig. 2), but distinct from possible mixing relations, which would likely not be linear on a log-log plot. This suggests that the Re-Os systematics of most IVA irons were produced during core crystallization, not by mixing native metal with projectile metal.

According to Scott *et al.* (*18*), Duel Hill, which shows the largest deviation from the isochron, does not fit their IVA crystallization model for most trace element trends. The pronounced deviation in the Re-Os isotope system may imply that Duel Hill (1854) does not belong to the main crystallization sequence of the IVA parent body. In contrast, La Grange and Bushman Land are compositionally consistent with the common trace element trends in the IVA group. They plot within error of the older isochron defined by the IIA irons (Fig. 1C). Their deviation from the IVA isochron may reflect formation in isolated melt reservoirs with separate cooling histories. For example, Rasmussen *et al.* (*17*) reported that the IVA irons can be divided into subgroups that show substantially different average cooling rates. Distinct Re-Os isotopic behavior could result from partial melting of a core if melts are produced in two or more chemically distinct domains within the core: one domain that evolved before the impact with a high Re/Os ratio, and another domain with a low Re/Os ratio. Our sample set, however, has minimal overlap with the set of Rasmussen *et al.* (*17*), so it is not yet known if the Re-Os systematics reflect a difference between slow-cooling and fast-cooling IVA irons.

Another factor complicates the direct interpretation of the IVA correlation line as an isochron. Chen and Wasserburg reported ^{107}Pd-^{107}Ag systematics of several IVA irons to be consistent with crystallization within 10 My of nucleosynthesis (*7*), a result inconsistent with such a young Re-Os isochron age. The difference in slope between our IIIA and IVA isochrons implies at least a 56-My difference in age. Thus, the interpretation of the IVA isochron as a primary crystallization age is in direct contradiction with Pd-Ag results. If the Re-Os age reflects a secondary melting and crystallization event, the results may indicate that the Pd-Ag systematics somehow survived this event.

The IVB samples show a limited variation in $^{187}\text{Re}/^{188}\text{Os}$—only about 12% of the range in the IIA group. Consequently, IVB data define a less precise isochron (Fig. 1D). The confidence limits of the IVB isochron

Table 1. Re and Os data for IIA, IIIA, IVB, and IVA iron meteorites. Uncertainties for the $^{187}\text{Re}/^{188}\text{Os}$ and $^{187}\text{Os}/^{188}\text{Os}$ ratios are 2σ and refer to the last decimal places. Uncertainties for the $^{187}\text{Re}/^{188}\text{Os}$ ratio take into account both isotope dilution error and variability in blank contribution. Abbreviations: USNM, U.S. National Museum of Natural History; KMAN, Committee on Meteorites, Russian Academy of Sciences; ppb, parts per billion.

Sample	Source	Weight (g)	Re (ppb)	Os (ppb)	$^{187}\text{Os}/^{188}\text{Os}$	$^{187}\text{Re}/^{188}\text{Os}$
			IIA group			
Lombard	USNM-1684	0.5513	156.7	767.3	0.173069± 39	0.9896±17
Filomena	USNM-1334	0.1591	201.8	1036.5	0.169284± 36	0.9431±34
Replicate		0.1701	201.7	1038.7	0.169307± 43	0.9405±33
Replicate		0.1628	201.6	1040.1	0.169265± 47	0.9389±33
Replicate		0.2577	201.8	1040.6	0.169173± 42	0.9393±28
Gressk	KMAN-15674	0.1209	515.3	3389.4	0.153185± 28	0.7349±20
Replicate		0.2434	514.1	3386.3	0.153132± 18	0.7339±12
Coahuila	USNM-3298	0.1090	1242.8	10222	0.141467± 17	0.5869±14
Bennett County	USNM-1199	0.0540	4532.2	57616	0.125160± 17	0.3789± 6
Negrillos	USNM-1222	0.0738	4838.9	65696	0.123304± 17	0.3547± 6
			IIIA group			
Charcas	Paris	0.2616	150.6	1095.8	0.147634± 27	0.6638±15
Replicate		0.3612	150.8	1091.8	0.147795± 24	0.6671±12
Susuman	KMAN-2293	0.2278	156.2	1128.4	0.148054± 30	0.6688±17
Replicate		0.3527	155.8	1125.6	0.148062± 41	0.6686±12
Ssyromolotovo	KMAN-65	0.2687	307.9	2459.9	0.142874± 18	0.6044±12
Loreto	USNM-1507	0.1865	376.7	3755.4	0.133413± 20	0.4835± 8
Casas Grandes	USNM-369	0.1085	403.8	3800.9	0.135612± 31	0.5124± 9
Toubil River	KMAN-627	0.2225	426.0	3815.2	0.137662± 37	0.5387±10
Replicate		0.1575	426.6	3831.6	0.137656± 36	0.5371±12
Henbury	USNM-6494	0.1913	1327.7	15439	0.127907± 20	0.4144± 7
Replicate		0.1714	1324.1	15390	0.127929± 18	0.4145± 7
Costilla Peak	USNM-720	0.1265	1428.6	18629	0.124409± 29	0.3693± 6
			IVA group			
Duel Hill (1854)	USNM-52	1.5544	34.60	244.1	0.149832±102	0.6848±13
Duchesne	USNM-2181	1.1174	35.34	249.5	0.148708± 31	0.6844±14
New Westville	USNM-1412	0.4229	44.60	319.2	0.147928± 58	0.6751±21
Bushman Land	USNM-2515	0.6040	114.7	998.3	0.138940± 22	0.5545±10
Charlotte	USNM-577	0.2803	203.6	1957.2	0.134652± 25	0.5016± 9
Gibeon	USNM-3768	0.2353	271.6	2773.7	0.132235± 34	0.4720± 8
La Grange	USNM-55	0.3306	288.3	3037.3	0.131408± 22	0.4576± 7
Yanhuitlan	USNM-459	0.2336	349.5	3839.5	0.129754± 17	0.4386± 8
Maria Elena	USNM-1221	0.2885	349.9	3804.2	0.130001± 39	0.4433± 9
Jamestown	USNM-1046	0.2195	385.6	4360.3	0.128830±137	0.4261± 7
			IVB group			
Warburton Range	USNM-5884	0.1364	1303.1	15702	0.126896± 10	0.3998± 6
Tawallah Valley	USNM-1458	0.1654	1386.6	16894	0.126580± 22	0.3954± 6
Weaver Mountain	USNM-3145	0.0992	1493.4	18497	0.126097± 59	0.3889± 6
Replicate		0.1139	1493.3	18469	0.126097± 14	0.3895± 6
Hoba	USNM-6506	0.1761	2757.3	39391	0.121947± 33	0.3370± 5
Tlacotepec	USNM-872	0.0984	3165.9	47007	0.120944± 52	0.3242± 5
Replicate		0.1017	3168.2	47030	0.121027± 23	0.3243± 5
Cape of Good Hope	USNM-985	0.1175	3271.7	48743	0.120945± 56	0.3231± 5
Replicate		0.1604	3270.4	48623	0.120949± 21	0.3238± 5

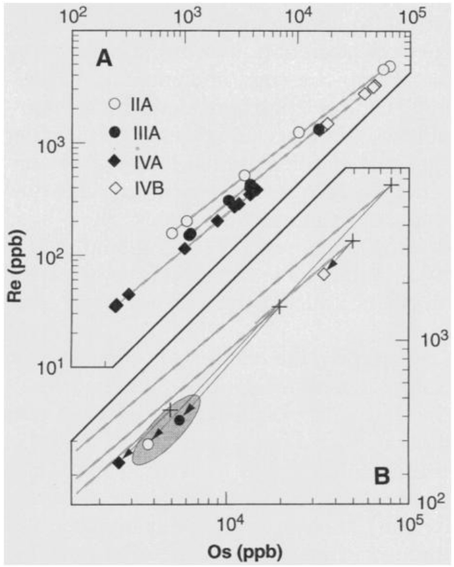

Fig. 2. Re and Os crystallization trends in magmatic irons. (**A**) The symbols represent the experimental data for each group, and the gray lines show fractional crystallization sequences calculated with distribution coefficients from (*20*). (**B**) Enlargement of a portion of the plot in (A) showing the modeling of the initial melt composition. Gray lines show the same crystallization sequences as in (A), and crosses represent the compositions of the first crystals for the corresponding group. Calculated initial melt compositions for each group are shown in symbols following the legend in (A), and the gray ellipse shows the composition of chondritic metal (*21*); ppb, parts per billion.

Table 2. Regression results for IIA, IIIA, IVA, and IVB iron meteorites. Isochron treatment was accomplished by using Isoplot (*27*) with Model I fits. Uncertainties for the slope and $^{187}Os/^{188}Os$ initial ratios (I_O) are 95% confidence limits and refer to the last decimal places. Ages were calculated with the assumption that $\lambda(^{187}Re) = 1.666 \times 10^{-11}$ year^{-1}. Errors in age reflect only uncertainties in the slope of the isochron. MSWD, mean squared weight deviation.

Group	I_O	Slope	Age (Ma)	MSWD
IIA	0.09544 ± 7	0.07851 ± 14	4537 ± 8	1.15
IIIA	0.09524 ± 11	0.07887 ± 22	4558 ± 12	1.47
IVA	0.09584 ± 23	0.07721 ± 46	4464 ± 26	1.57
IVB	0.09559 ± 19	0.07834 ± 52	4527 ± 29	1.44

age overlap with the ages of both the IIA and IIIA isochrons (Table 2). These three groups, however, are resolvable in the Os isotope evolution diagram (Fig. 3): The IVB error ellipse plots distinctly above the IIA and IIIA ellipses.

On an age versus initial ratio plot (Fig. 3), the IIA, IIIA, and IVA isochrons define an Os isotope evolution line for the precursor reservoirs of their parent bodies. The slope of this line corresponds to a $^{187}Re/^{188}Os$ of 0.42 ± 0.06, which is identical within error to that of H chondrites (*19*), implying that this line may represent Os isotope evolution in the solar nebula. This result is consistent with the interpretation of the IVA isochron as a crystallization age. The fact that the IVB isochron (Fig. 3) plots above the chondritic evolution path indicates that the IVB precursor had a distinctly elevated $^{187}Os/^{188}Os$ ratio relative to the assumed value for the bulk solar nebula.

The high-precision Re and Os abundance data permit additional constraints to be placed on the formation of the parent bodies. All four groups form resolvable linear trends on log [Re] versus log [Os] plots (Fig. 2A). The slopes of these lines are related by the following equation: slope = $(k_{Re} - 1)/(k_{Os} - 1)$, where k_{Re} and k_{Os} are the metal solid–metal liquid distribution coefficients for Re and Os. These correlations allow us to calculate k_{Re} and k_{Os} and to model the initial parental melt composition for each group (Fig. 2B) (*20*). Modeling results suggest that the parental melts for IIA, IIIA, and IVA meteorites had Re and Os concentrations similar to their concentrations in chondritic metal (*21*). In contrast, the IVB group was evidently derived from a precursor with concentrations of Re and Os at least 10 times those of chondrite metal, and a Re/Os ratio distinctly lower than that of ordinary chondrites (*20*). This may imply that the IVB precursor material condensed from the solar nebula at higher temperatures (*22*). The subchondritic Re/Os ratio may then reflect a somewhat higher condensation temperature for Os than for Re.

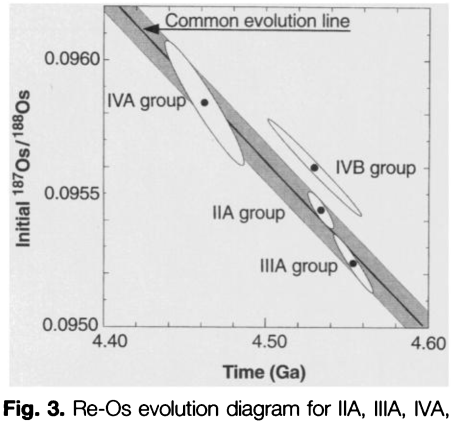

Fig. 3. Re-Os evolution diagram for IIA, IIIA, IVA, and IVB iron meteorites. Ellipses represent the 95% confidence areas for corresponding isochrons. Ellipses were calculated as described in (*28*). The gray line is the best fit for the IIIA, IIA, and IVA isochrons; it shows the Os isotopic evolution of their common reservoir. Ga, billions of years ago.

The Re-Os results indicate that all four cores crystallized early in the history of the solar system but that there were resolvable differences in the timing of the crystallization events. There is no overlap between the IIA, IIIA, and IVA iron meteorite isochrons. The IIA irons apparently became a system closed to the migration of Re and Os anywhere from about 1 to 40 My subsequent to the IIIA system. The IVA irons, in contrast, became a closed system about 100 My after the IIIA system. These age differences may reflect the size of the planetary body (hence cooling rate), record different formation ages of the parent bodies, or perhaps in the case of the IVA irons, record a remelting and crystallization event. Consequently, the chondritic evolution of the initial isotopic compositions may indicate either formation of the cores from planetesimals of variable size that had grossly chondritic Re/Os, or that the planetesimals were sequentially constructed from nebular materials with chondritic Re/Os. The isochron results for the IVB irons indicate crystallization at approximately the same time as the IIA and IIIA irons, but with a distinctly higher initial $^{187}Os/^{188}Os$ ratio. Because of the very limited amount of time available to evolve an ^{187}Os-enriched reservoir, the higher initial ratio suggests significant Os isotopic inhomogeneity in the solar nebula.

REFERENCES AND NOTES

1. E. R. D. Scott, *Geochim. Cosmochim Acta* **36**, 1205 (1972).
2. J. W. Morgan, M. F. Horan, R. J. Walker, J. N. Grossman, *ibid.* **59**, 2331 (1995); *Meteoritics*, in press.
3. L. E. Nyquist, B. Bansal, H. Wiesman, C. Y. Shih, *Meteoritics* **29**, 872 (1994).
4. I. D. Hutcheon and E. Olsen, *Lunar Planet. Sci.* **22**, 605 (1991); I. D. Hutcheon, E. Olsen, J. Zipfel, G. J. Wasserburg, *ibid.* **23**, 565 (1992).
5. W. R. Kelly and G. J. Wasserburg, *Geophys. Res. Lett.* **5**, 1078 (1978); T. Kaiser and G. J. Wasserburg, *Geochim. Cosmochim. Acta* **42**, 43 (1978).
6. J. H. Chen and G. J. Wasserburg, *Geochim. Cosmochim. Acta* **47**, 1725 (1983); *ibid.* **54**, 1729 (1990); *Earth Planet. Sci. Lett.* **52**, 1 (1981).
7. ———, *J. Geophys. Res.*, in press.
8. M. F. Horan, J. W. Morgan, R. J. Walker, J. N. Grossman, *Science* **255**, 1118 (1992).
9. J. J. Shen, D. A. Papanastassiou, G. J. Wasserburg, *Lunar Planet. Sci.* **26**, 1283 (1995).
10. M. I. Smoliar, R. J. Walker, J. W. Morgan, S. B. Shirey, *ibid.*, p. 1323.
11. M. Lindner, D. A. Leich, G. P. Russ, J. M. Bazan, R. J. Borg, *Geochim. Cosmochim. Acta* **53**, 1597 (1989).
12. D. A. Papanastassiou, H. H. Ngo, G. J. Wasserburg, *Lunar Planet. Sci.* **25**, 1041 (1994).
13. G. W. Lugmair and S. J. G. Galer, *Geochim. Cosmochim. Acta* **56**, 1673 (1992).
14. G. W. Lugmair, C. MacIsaak, A. Shukolyukov, *Lunar Planet. Sci.* **23**, 823 (1992).
15. Unlike previous studies (*2*, *23*), our work here used a mixed Re-Os spike, and we equilibrated the spikes and standards with aqua regia in sealed glass tubes by heating to 240°C. The mixed Re-Os spike was calibrated against the same Re and Os standard solutions used in our previous studies. To check the reproducibility of this procedure, we analyzed multiple pieces of the IIA iron Filomena. Samples were cut from a single piece of the meteorite as adjacent chunks. Four chunks were leached before analysis with 0.8 M HNO_3, removing ~5% by weight of the iron. For these samples, Os concentration and isotopic composition data varied little. In contrast, Re abundances varied by ±2%, suggesting that the Re was not consistently removed with the leachate. Four other chunks were cleaned mechanically without leaching. For these chunks, reproducibility was quite good for Re and Os concentrations, with a total Re/Os uncertainty of ±0.2% and an $^{187}Os/^{188}Os$ uncertainty of ±0.034%. This result indicates that Re may be redepositing during leaching, producing a systematic error in the Re/Os ratio. Therefore, all samples in this study were cleaned mechanically without leaching and washed with pure alcohol in an ultrasonic bath. These improvements have led to a factor of 2 reduction in Re/Os uncertainty relative to our previous techniques (*2*) and have enabled us to measure group IIA and IIIA irons with higher precision. We estimate 2σ precision for $^{187}Os/^{188}Os$ and $^{187}Re/^{188}Os$ ratios to be generally better than ±0.05 and ±0.3%, respectively. Total analytical blanks for this study, including loading and filament blanks, averaged 40 pg for Re and 3 pg for Os. These blank amounts are well below the >50 ng of Re and >370 ng of Os processed for each sample and should not significantly increase the errors in our measurements.
16. If the assumption is correct that the age of the IIIAB irons is within ±5 My (0.11%) of the age of angrites, then the low uncertainty in the slope of the IIIA isochron [0.07887 ± 0.00022 (0.29%)] permits a refinement of $\lambda(^{187}Re)$ to ±0.31%. This is true only for our particular spike solution, because the spike calibration presumably included a systematic error due to nonstochiometry of the Os salt we used as a standard. Morgan *et al.* (*2*) estimated that the $(NH_4)_2OsCl_6$ standard used here is stoichiometric to within ~1.2%. We also note that our IIA isochron and Os concentration data coincide well with the

results of Shen *et al.* (*8*), who independently calibrated their spikes. Consequently, we recommend a refined value for $\lambda(^{187}\mathrm{Re})$ of $(1.666 \pm 0.017) \times 10^{-11}$ year^{-1}.

17. K. L. Rasmussen, F. Ulff-Møller, H. Haack, *Geochim. Cosmochim Acta* **59**, 2049 (1995).
18. E. R. D. Scott, H. Haack, T. McCoy, *ibid.*, in press.
19. R. J. Walker, J. W. Morgan, M. F. Horan, G. N. Grossman, *Lunar Planet. Sci.* **24**, 1477 (1993).
20. The partitioning of refractory elements between metallic solid and metallic melt in Fe-Ni systems is strongly dependent on the S (and P) content of the parental melts. Because of the limited experimental data for the correlation of k_{Re} and k_{Os} with S concentration (*24*), we calculated the Re and Os distribution coefficients as follows. We assumed k_{Ir} in IIA, IIIA, IVA, and IVB groups as 20, 3.5, 1.7, and 1.3, respectively, on the basis of the correlation of k_{Ir} with S concentration from (*25*). Using Ir abundances from (*26*) and our Os data, we calculated k_{Os} from the slopes of Os-Ir lines [slope = $(k_{\mathrm{Ir}} - 1)/(k_{\mathrm{Os}} - 1)$]. Similarly, k_{Re}'s were calculated from slopes of Re-Os lines. This procedure gave the following distribution coefficients: for Os, 28, 4.5, 2.0, 1.4; and for Re, 22, 3.8, 1.8, 1.3 in the IIA, IIIA, IVA, and IVB groups, respectively. To calculate the parental melt compositions, we assumed that the Re and Os abundances in the first crystals to form from each melt were equal to their abundances in those meteorites with the highest Os (or Ir) concentrations [Negrillos (IIA), Costilla Peak (IIIA), Jamestown (IVA), Cape of Good Hope (IVB)]. From these concentrations and the above calculated k_{Re} and k_{Os}, the following parental melt concentrations (in parts per billion) are obtained for Re and Os, correspondingly: 220, 2380 (IIA); 380, 4140 (IIIA); 210, 2200 (IVA); 2440, 34300 (IVB).
21. E. R. Rambaldi, *Earth Planet. Sci. Lett.* **36**, 347 (1977).
22. W. R. Kelly and J. W. Larimer, *Geochim. Cosmochim. Acta* **41**, 93 (1977).
23. S. B. Shirey and R. J. Walker, *Anal. Chem.* **34**, 2136 (1995).
24. J. H. Jones and D. J. Malvin, *Metall. Trans. B* **21B**, 697 (1990); J. H. Jones and A. J. G. Jurewicz, *Eos* **75**, 694 (1994).
25. J. H. Jones and M. J. Drake, *Geochim. Cosmochim. Acta* **47**, 1199 (1983).
26. J. T. Wasson, X. Ouyang, J. Wang, E. Jerde, *Geochim. Cosmochim. Acta* **53**, 735 (1989), and references therein.
27. K. Ludwig, *U.S. Geol. Surv. Open File Rep. OF 88-0557* (1988).
28. J.-F. Minster, L.-P. Ricard, C. J. Allegré, *Earth Planet. Sci. Lett.* **44**, 420 (1979).

29. We thank R. S. Clarke, M. Ivanova, and J. T. Wasson for meteorite samples. Comments by R. W. Carlson and two anonymous reviewers helped to improve this manuscript. Supported by National Aeronautics and Space Administration grant NAGW 3625 and by Geological Society of America Student Research grant 5710-95.

4 August 1995; accepted 27 November 1995

The Swelling of Clays: Molecular Simulations of the Hydration of Montmorillonite

S. Karaborni,* B. Smit, W. Heidug, J. Urai, E. van Oort

The swelling of clay minerals on contact with an aqueous solution can produce strong adverse effects in the exploration and production of gas and oil. Molecular dynamics and Monte Carlo simulations were used to study the mechanism of swelling of sodium-montmorillonite. The simulations showed that the abundant clay mineral has four stable states at basal spacings of 9.7, 12.0, 15.5, and 18.3 angstroms, respectively. The amount of swelling and the locations of the stable states of sodium-montmorillonite are in good quantitative agreement with the experimental data.

Clays are important in many applications, such as drug and agrochemical delivery, purification and recycling of water streams, geological disposal of radioactive wastes, catalysis and catalysis support, and cosmetics. In the context of oil and gas production, swelling in clays is an important factor when drilling wells through mudrocks. The drilling engineer must ensure, through the use of drilling fluids, that the stresses induced in the region near the boreholes do not exceed the strength of the mudrock. Excessive stress could lead to severe drilling problems and even to the collapse of a well (*1*). Growing environmental concerns currently require the replacement of oil-based drilling fluids by more benign water-based solutions. The development of such high-performance fluids requires a molecular insight into the factors that control the swelling of clays.

Clays have a characteristic layered structure. Between these layers, water can adsorb, which results in strong repulsive forces that cause the clays to expand to as much as several times their original thickness (*2*). Clay hydration studies have been conducted since 1933 (*3*), yet there is no clear understanding of the swelling mechanism. We report here on our simulation results for a montmorillonite clay that is of interest to the drilling industry because of its strong tendency to swell (*1*). Molecular simulations were performed in the grand-canonical ensemble (*4*, *5*), that is, at constant chemical potential, volume, and temperature (μ, V, and T, respectively). The simulations modeled a typical experiment with a surface force apparatus in which the force is measured as a function of a fixed separation, for example, between two mica sheets immersed in water (*2*). In our simulations, the distance between the clay layers was fixed after each incremental increase in the interlayer distance, and the system was allowed to take or reject water molecules until equilibrium was reached. Initial tests of our simulation code, which is a combination of molecular dynamics and Monte Carlo techniques, showed that the interlayer water could reach very high densities. The random insertion of a water molecule into a dense system is difficult, and therefore the equilibration step is extremely lengthy. To facilitate the insertion of water molecules, we used the orientational-bias Monte Carlo technique (*6*, *7*).

Sodium-montmorillonite (Na-Mt) clays from different regions of the world have slightly different chemical structures and charge distributions. Our model for Na-Mt, water, and ions is similar to that developed from ab initio calculations by Skipper and

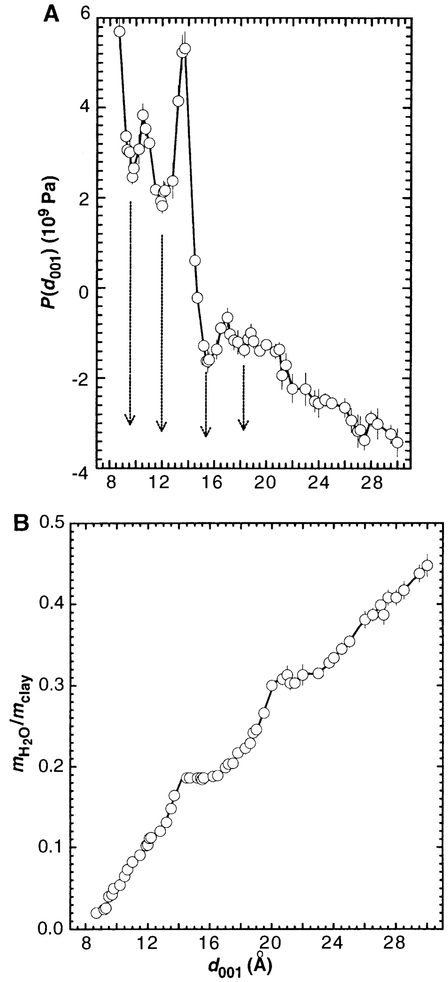

Fig. 1. Average simulated properties of Na-Mt as a function of basal spacing d_{001}. (**A**) Disjoining pressure $P(d_{001})$. (**B**) Ratio of water weight to clay weight, m_{H_2O}/m_{clay}, in units of grams per gram.

S. Karaborni and B. Smit, Koninklijke/Shell-Laboratorium, Amsterdam (Shell Research BV), P.O. Box 38000, 1030 BN Amsterdam, Netherlands.
W. Heidug, J. Urai, E. van Oort, Koninklijke/Shell Exploration and Production Laboratory, Volmerlaan 6, 2280 AB Rijswijk, Netherlands.

*To whom correspondence should be addressed.